Intracellular transport of insulin granules is a subordinated random walk

S. M. Ali Tabei[a,1], Stanislav Burov[a,1], Hee Y. Kim[a,b,c,1], Andrey Kuznetsov[d], Toan Huynh[a,b,c], Justin Jureller[c], Louis H. Philipson[d], Aaron R. Dinner[a,b,c,2,3], and Norbert F. Scherer[a,b,c,2,3]

[a]James Franck Institute, Departments of [b]Chemistry and [d]Medicine, and [c]Institute for Biophysical Dynamics, University of Chicago, Chicago, IL 60637

Edited by David A. Weitz, Harvard University, Cambridge, MA, and approved February 5, 2013 (received for review December 19, 2012)

We quantitatively analyzed particle tracking data on insulin granules expressing fluorescent fusion proteins in MIN6 cells to better understand the motions contributing to intracellular transport and, more generally, the means for characterizing systems far from equilibrium. Care was taken to ensure that the statistics reflected intrinsic features of the individual granules rather than details of the measurement and overall cell state. We find anomalous diffusion. Interpreting such data conventionally requires assuming that a process is either ergodic with particles working against fluctuating obstacles (fractional Brownian motion) or nonergodic with a broad distribution of dwell times for traps (continuous-time random walk). However, we find that statistical tests based on these two models give conflicting results. We resolve this issue by introducing a subordinated scheme in which particles in cages with random dwell times undergo correlated motions owing to interactions with a fluctuating environment. We relate this picture to the underlying microtubule structure by imaging in the presence of vinblastine. Our results provide a simple physical picture for how diverse pools of insulin granules and, in turn, biphasic secretion could arise.

pancreatic beta-cells | subdiffusive motion | steered transition path sampling | detrended fluctuation analysis

Eukaryotic cells package proteins into vesicles for trafficking and spatially localized secretion. These essential functions are highly regulated, and defects in them can lead to disease (1, 2). Although optical microscopy, combined with molecular and cellular biology, can provide important insight into intracellular dynamics, in the past, most measurements detected variations in intensities from many molecular events and thus averaged in some way. These include fluorescence correlation spectroscopy (FCS) (3), fluorescence recovery after photobleaching (FRAP) (4), and image correlation spectroscopy (5). Recent advances in experimental methods now enable tracking single particles in cells (6). Although these measurements still involve a degree of time averaging (7), the resulting individual time trajectories contain more information than the mean values extracted from the aforementioned approaches.

Qualitatively, the time trajectories reveal complex behaviors: combinations of random, directed, transiently stalled and constrained motions (e.g., refs. 7, 8). These different types of motion reflect the interplay of various molecular components in crowded environments. Quantifying their relative importance can constrain mechanisms, but extracting this information from the particle tracking data requires new theoretical tools. Operationally, one strategy is to classify segments of trajectories according to their motions (e.g., active and passive) (9, 10), but this requires long trajectories. A less data-demanding approach is to identify different types of anomalous diffusion (11).

What features can give rise to the observed anomalous behavior? Simple crowding is insufficient, as it results in standard Brownian motion but with a reduced diffusion coefficient (12). Instead, anomalous behavior implies a form of heterogeneity. The random steps can be broadly distributed in time, leading to a continuous-time random walk (CTRW) (13), or in space, leading to fractional Brownian motion (FBM) (14). Various statistical tests have been introduced to distinguish these universality classes from each other and from simple Brownian motion (i.e., a random walk with homogeneous steps in time and space) (15).

Several studies have applied these tests to subdiffusive dynamics in cells. The earliest considered only FBM (7, 16). More recent ones allowed for both FBM and CTRW (17, 18) and found that the two models contribute to varying extents depending on the system: The motion of bacterial chromosomal loci was almost pure FBM (18), whereas the diffusion of the Kv2.1 potassium channel in the plasma membrane of human embryonic kidney cells was found to combine ergodic (FBM) and nonergodic (CTRW) processes. Given these two very different examples, it is important to examine other forms of intracellular transport to elucidate statistical signatures of molecular mechanisms and to understand how the motions relate to biological function.

We use spinning-disk confocal microscopy and particle tracking to obtain trajectories of individual insulin-containing vesicles, termed granules, in cells. Pancreatic β-cells package the hormone insulin into granules (250–350 nm in diameter) and traffic it to the plasma membrane to enable rapid release in response to glucose stimulation. Failure of secretion is associated with type 2 diabetes. Biphasic insulin secretion, composed of a fast release followed by a slower second phase, is disturbed in the advancing diabetic state with (initially) progressive loss of the first phase (19). Different pools of granules and membrane docking scenarios have been suggested to underlie biphasic secretion based on qualitative analysis of limited numbers of granules, but these features remain poorly defined despite much effort to observe them in β-cells (20).

We labeled insulin granules using a syncollin-GFP construct that was targeted to them following transfection (21). We observe anomalous diffusion in the granule transport in MIN6 insulinoma cells and find that it satisfies tests for both FBM and CTRW. In other words, the random steps are characterized by heterogeneity in both space and time. Care is taken to ensure that nonergodic behavior reflects intrinsic features of the granule motion rather than changes in cell state. We show that a simple model that combines FBM and CTRW through subordination accounts for all of the observations. Analysis of the granule motion in the presence of vinblastine, a microtubule-disrupting drug, allows us to relate the dynamics to the structure of the microtubule network. We also present simulations showing that our kinetic scheme can account for the otherwise unexplained apparent granule storage pools and biphasic secretion of insulin.

Author contributions: L.H.P., A.R.D., and N.F.S. designed research; S.M.A.T., S.B., H.Y.K., and T.H. performed research; A.K. and J.J. contributed new reagents/analytic tools; S.M.A.T. and S.B. analyzed data; and S.M.A.T., S.B., L.H.P., A.R.D., and N.F.S. wrote the paper.

The authors declare no conflict of interest.

This article is a PNAS Direct Submission.

[1]S.M.A.T., S.B., and H.Y.K. contributed equally to this work.

[2]A.R.D. and N.F.S. contributed equally to this work.

[3]To whom correspondence may be addressed. E-mail: dinner@uchicago.edu or nfschere@uchicago.edu.

This article contains supporting information online at www.pnas.org/lookup/suppl/doi:10.1073/pnas.1221962110/-/DCSupplemental.

Results and Discussion

Anomalous Diffusion of Insulin Granules. We study MIN6 cells because they have about 10-fold fewer granules than wild-type mouse β-cells, which allows resolving and tracking hundreds of individual granules. The reduced density also mitigates granule–granule crowding effects. In Fig. 1*A*, we show a typical MIN6 cell expressing syncollin-GFP in the insulin granules. The fluorescently labeled insulin granules are dispersed throughout it. The distribution of displacements has non-Gaussian statistics (Fig. 1*B*), and the trajectories appear to have a wide range of behaviors (*SI Appendix*, Fig. S1). As a first step toward characterizing the type of motion performed by the granules, we calculate the time-averaged mean square displacement (TA-MSD) (4, 7, 8, 22–24) for each single-granule trajectory as

$$\overline{\delta(s,t)^2} = \frac{1}{t-s}\int_0^{t-s} \left[r(\tau+s)-r(\tau)\right]^2 d\tau, \qquad [1]$$

where r is the position of the particle, s is the lag time, and t is the total measurement time for each trajectory. Throughout this paper, we use overlines to indicate time averages and angle brackets to denote ensemble averages. The TA-MSD can be viewed as a moving-average analysis. Fig. 2*A* shows the TA-MSD. Unless otherwise indicated, the data are from a single representative cell, and we use only the 186 trajectories with at least 200 observation points (spaced at 1-s intervals); data for additional cells are shown in *SI Appendix*, Fig. S2. As the time lag s increases, the range available for averaging decreases, so we observe increasing sampling noise as s approaches 100 s.

The exponent α in the scaling relation $\delta^2 = Ds^\alpha$ characterizes the motion: $\alpha = 1$ for pure diffusive (Brownian) motion, $\alpha < 1$ for subdiffusive motion, $\alpha > 1$ for superdiffusive motion, with $\alpha = 2$ corresponding to pure ballistic motion. The overall trend in Fig. 2*A* is subdiffusive, with $\alpha = 0.76$. Fig. 2*A* also shows that the TA-MSDs of the trajectories are distributed and the anomalous diffusion coefficient D exhibits a broad variation. When the exponent α is calculated by fitting to the first 10% of the data points of the individual trajectories, we find the distribution to be broader than expected from intrinsic randomness or regular spatial inhomogeneities; the values of α span from the subdiffusive to superdiffusive regimes, whereas the mean is at $\alpha = 0.76$ (*SI Appendix*, Fig. S3).

Going beyond the standard TA-MSD analysis, Fig. 1*B*, *Inset* shows the distribution of the x components of the spatial displacements between successive 1-s time intervals; similar behavior is observed for the y components. The distribution is clearly non-Gaussian with long tails that represent the enhanced probability of the granules making large displacements. To make this

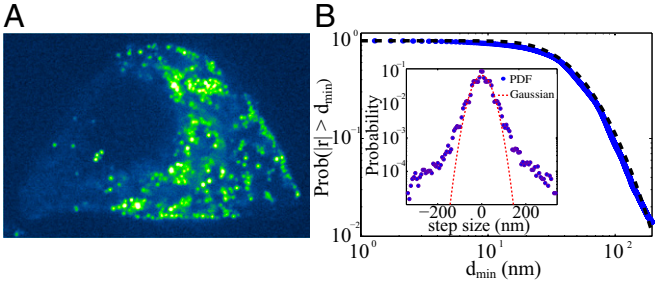

Fig. 1. (*A*) Typical confocal fluorescence image of syncolin-EGFP–labeled insulin granules in live MIN6 cells. Granules are typically 350–400 nm in diameter. See *SI Appendix*, Fig. S1, and Movie S1 for examples of trajectories. (*B*) Cumulative distribution of jump lengths (symbols) and fit of an integrated log-normal distribution (dashed line). (*Inset*) Raw distribution of x components of steps compared with a Gaussian fit.

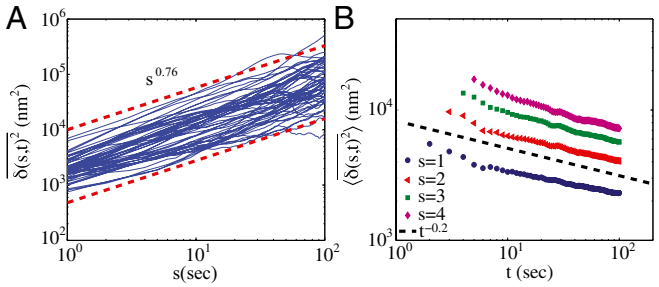

Fig. 2. (*A* and *B*) Time-averaged mean square displacement (TA-MSD) as a function of lag time s (*A*) and measurement time t (*B*); see Eq. **1** and main text. In *A*, the blue lines are for individual trajectories of length $t = 200$ s, and the red dashed lines show an exponent of $\alpha = 0.76$. In *B*, the lines are averaged over the same set of trajectories, with s as indicated.

observation more precise, we plot the distribution of granule displacements, $P(\delta)$, for various time intervals, s, in *SI Appendix*, Fig. S4. Here, $\delta(s) = |r(\tau+s) - r(\tau)|$, where we have averaged over τ. For a system obeying Gaussian statistics, it is expected that $P(\delta)$ would depend only on the second moment $\sigma^2 = \langle \delta(s)^2 \rangle$. We determined whether $P(\delta)$ for the granule data obeys Gaussian statistics for different values of s. For Brownian motion, one expects a collapse of $P(\delta)$ for different s to a single curve when normalized by σ. However, this is clearly not the case for the granule data (*SI Appendix*, Fig. S4). We also measured the distribution of different jump lengths during the motion. Fig. 1*B* shows the cumulative distribution of different jump lengths, i.e., the probability to perform a jump larger than $d_{\min}$. The data are fitted well by a log-normal distribution, suggesting uncorrelated processes with multiplicative probabilities.

It is also important to establish whether the granule dynamics exhibit ergodic behavior. This is accomplished by changing the extent of data used for each trajectory (t in Eq. **1**) and by measuring the value of $\langle \delta^2(s,t) \rangle$ for a constant s. For this analysis, we first time average each trajectory and then average over the ensemble of granules. For a system that obeys ergodic behavior one expects the time and ensemble averages to converge at long times. In striking contrast, Fig. 2*B* shows that $\langle \delta^2(s,t) \rangle$ decays as a power law for increasing t. The observed motion is not ergodic, and the statistic reveals ever deeper traps as more data are included. This behavior is called "aging" in the literature on glasses (25). It is important to emphasize that aging is an ongoing intrinsic feature of the motion, not a result of a change in cell state.

Competing Forms of Subdiffusive Behavior. Finding that the movement of granules inside the β-cells is anomalous, non-Gaussian, and nonergodic motivates us to characterize those observations in the framework of two standard models of anomalous diffusion: FBM and CTRW. These two models differ with respect to their physical motivations. In a CTRW model, the motion is described by a particle that jumps between traps with random dwell times; the distribution of dwell times follows a power law $t^{-\beta-1}$ with $0 < \beta < 1$. The motion is annealed, which means that, when the particle returns to the same trap, the waiting time is different. In CTRW, the spatial step sizes are usually assumed to be uniform. The net effect is that the system is nonergodic with a broad scatter of single-trajectory TA-MSDs that average to be linear in s (26, 27). The system is nonergodic because deeper and deeper traps are discovered the longer one measures. In our system, the traps could correspond to binding events with a distribution of dissociation times or cages with varying lifetimes.

In contrast, FBM is a Gaussian stationary process. The spatial position $x(t)$ is correlated such that $\langle x(t)x(t+s) \rangle \propto (|t|^{2H} + |t+s|^{2H} - |s|^{2H})$, where H is the Hurst exponent (15, 28). The microscopic picture is not as transparent as CTRW. Simple examples

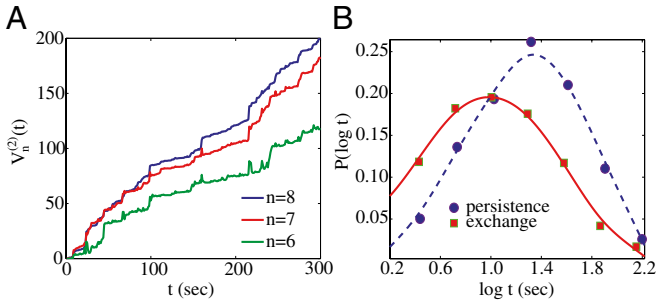

Fig. 3. Further tests for FBM and CTRW. (*A*) The 2-variation, $V_n^{(2)}(t)$, of a selected trajectory of length 300 s for $n = 6$, 7, and 8. (*B*) Decoupling of the persistence and exchange times. The minimum displacement threshold is 172 nm. Smooth curves are Gaussian fits to the logarithmic scale data.

yielding FBM statistics are diffusing particles interacting with random obstacles (e.g., as in single-file diffusion) (29) or diffusing particles that interact within a viscoelastic medium with a broad range of coupling strengths (30). In this case, the system is ergodic (i.e., there should be no dependence on measurement time), and one expects no scatter for the TA-MSD with a sublinear exponent.

Our goal is to determine the extent to which these models explain the subdiffusive statistics of the granule motion. There are a number of standard statistical measures for this purpose. The sublinear behavior of the TA-MSD (Fig. 2*A*) immediately suggests FBM with $H < 0.5$ (15, 28). A spatially bounded CTRW can also exhibit sublinear behavior (31) but can be excluded here owing to the difference in magnitude of the exponents in Fig. 2 *A* and *B*; they would be exact opposites of each other for a spatially bounded CTRW. To strengthen the connection to the FBM model, we also apply a test recently introduced to discriminate between FBM and CTRW (32): the *p*-variation ($V_n^{(p)}$). This measure divides a trajectory into 2^n segments; then, the scaling of the differences in position in successive segments is determined by summing over the differences raised to the p power. For CTRW, $V_n^{(2)}(t)$ saturates as n is increased, whereas for FBM, $V_n^{(2)}(t)$ diverges as $n \to \infty$. We estimated the 2-variation with some of our longest granule transport time series, and the trend shown in Fig. 3*A* favors FBM over CTRW.

At the same time, FBM is not sufficient to account for all of the observations. The broad scatter in Fig. 2*A* and the aging and lack of ergodicity in Fig. 2*B* suggest CTRW behavior. Interestingly, for long t in Fig. 2*B*, one observes convergence to a constant value, which suggests a cutoff time for the CTRW model. A lack of ergodicity can also be detected by decoupling of the distributions of persistence and exchange times (33–35). The persistence time is the time for a particle to first become mobile. Namely, if we consider a particle i, initially at $t_0 = 0$ with position $r_i(0)$, then the persistence time t_1 for a cutoff distance d is the first time that $|r_i(t_1) - r_i(0)| \geq d$. The exchange times are the subsequent times for moving this amount, such that $|r_i(t_n) - r_i(t_{n-1})| \geq d$ for $n > 1$. We observe decoupling for $50 < d < 300$ nm (Fig. 3*B*). The decoupling of the two distributions, as well as another ergodicity breaking parameter (26) (*SI Appendix*, Fig. S5), supports CTRW. The broad scatter of the TA-MSD for individual trajectories in Fig. 2*A* is consistent with nonergodicity and is discussed further in *SI Appendix* (26).

Unified Model. The statistical measures above suggest that the granule data contain FBM and CTRW features simultaneously, and there is a precedent for this possibility (17). Certainly the cellular environment is a dense viscoelastic medium (36, 37), and elastic-like coupling of granules to the cytoskeleton would be consistent with FBM. At the same time, granules can attach to microtubules through multiple motors, so that the binding and unbinding times could be sufficiently distributed to give rise to a CTRW. Thus, it is meaningful to consider a model that combines CTRW and FBM.

We developed a simple simulation to determine whether a hybrid model could account for all of the observed statistics. The simulation involves generating a sequence of random times distributed with a power law with exponent β and then, at each step, moving in one dimension by an amount consistent with a FBM spatial trajectory. The statistics of stochastic processes that subordinate an ergodic process (FBM) to a nonergodic process (CTRW) are known (38, 39). To make a better match between the one-dimensional hybrid model and the experimental trajectories we use the exponent equality $\alpha = 1 - \beta + 2H\beta$, where α is the exponent describing the sublinear behavior of the TA-MSD, $\beta - 1$ is the exponent of the aging power-law decay (*SI Appendix*), and H is the FBM Hurst exponent (39). To obtain $\alpha = 0.76$, as in Fig. 2*A*, we first match $\beta - 1$ to the experimental value in Fig. 2*B* and find $\beta - 1 = 0.2$; we then set $H = 0.35$ for the FBM process. The estimated β and H are consistent with the multiplicative behavior of the ensemble-averaged MSD exponent (*SI Appendix*, Fig. S6) (39). The simulation so defined gives results that are consistent with the granule data (i.e., compare Figs. 2 and 3 with Fig. 4 and *SI Appendix*, Fig. S5 with *SI Appendix*, Fig. S7). The success of the simple subordinated random walk simulation indicates that molecular models of intracellular transport should incorporate elements of both FBM and CTRW pictures.

Disruption of Microtubules Changes the Dynamics. To probe one aspect of the molecular basis for the observed anomalous behavior, we performed an analysis analogous to that described above for granule trajectories from cells that were subjected to the anticancer drug vinblastine. Vinblastine is known to influence insulin granule dynamics by affecting microtubules in a dose-dependent manner (40). At low concentrations, it prevents the growth and shortening of microtubules without causing net depolymerization. At high concentrations (micromolar), it causes depolymerization and leads to protofilament spirals and protein aggregates. We

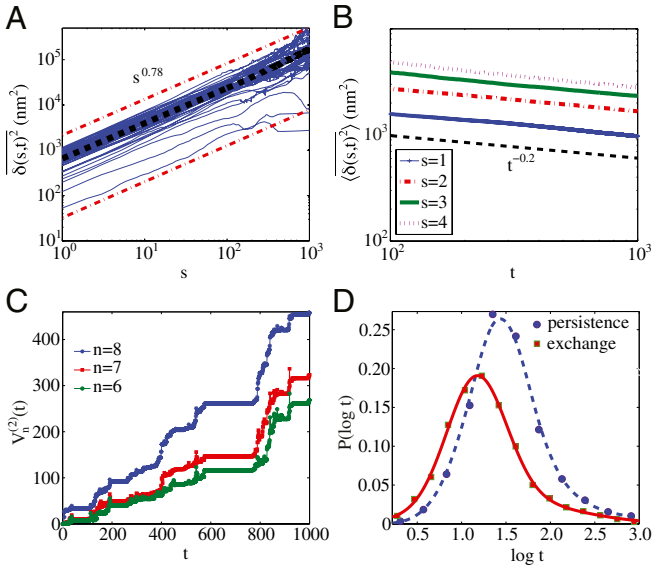

Fig. 4. Hybrid model in which FBM is subordinated to CTRW. (*A*) TA-MSD of the simulated trajectories with an overall sublinear trend of $s^{0.78}$ (compare with Fig. 2*A*). (*B*) Aging behavior consistent with Fig. 2*B*. (*C*) Two-variation of a sample trajectory for $n = 6$, 7, and 8 (compare with Fig. 3*A*). (*D*) Decoupling of persistence and exchange times (compare with Fig. 3*B*); smooth curves are Gaussian fits to the logarithmic scale data. The FBM trajectory was generated using the FBM library in Matlab with a Hurst exponent of $H = 0.35$.

treated MIN6 cells with 5 μM vinblastine and measured granule dynamics in live MIN6 cells at various times after exposure.

The TA-MSDs calculated from these data are again sublinear. As the exposure time to vinblastine increases, the exponent becomes progressively smaller until s is about 10 s (Fig. 5*A*). Then, at longer timescales, the TA-MSD exhibits a crossover to a much steeper trend ($\alpha = 1$). Analyzing the dependence on the measurement time (Fig. 5*B*), we find that aging shows power-law behavior at >10 s, with the same exponent as that of the untreated system ($\beta - 1 = -0.2$, Fig. 2*B*). Again, using $\alpha = 1 - \beta + 2H\beta$, we estimate the value of the FBM Hurst exponent at longer timescales to be $H = 0.5$, which is consistent with a memory-less behavior. Put together, these statistics indicate that, in the presence of vinblastine, FBM-type correlations in the motion are limited to 10 s, and beyond that timescale, the dynamics can be described as (memory-less) CTRW. This result contrasts with the effect of Swinholide A and Cytochalasin D in a potassium channel study that observed coexisting ergodic and nonergodic processes (17): In that case, the drugs, which disrupt the actin cytoskeleton, eliminated the CTRW component, restoring ergodicity.

We interpret our data as follows (see *SI Appendix*, Fig. S8 for a schematic). Motion at timescales less than 10 s is spatially correlated as in FBM, consistent with trafficking along microtubules. However, the filaments are shortened by the drug, and the overall network is reduced to localized disconnected and more crowded regions (Fig. 6 and *SI Appendix*, Figs. S9 and S10). Consequently, at longer timescales (and hence length scales), the transport of the granules between the disconnected regions is microtubule independent and is not correlated in time. It is interesting that the CTRW behavior persists, possibly due to the random waiting times between binding and unbinding of the granules to the microtubules between different regions. We reproduce this crossover with the hybrid model in *SI Appendix*, Fig. S11.

Microscopic Interpretation. The picture that emerges is that granule dynamics reflect both active and passive mechanisms as well as the dense cellular environment. The kinetic schemes identified can be used to delineate molecular hypotheses, and a reasonable scenario given our analysis is the following. The granules undergo transport on the microtubules and actin filaments via different molecular motors (41). These motors bind and unbind to microtubules and actin filaments, perform hops, and change the direction of their movement on the underlying pathways, which is a randomly cross-linked network. The distribution of waiting times giving rise to CTRW arises from random binding and unbinding times. The FBM contribution could originate from either the fluctuating

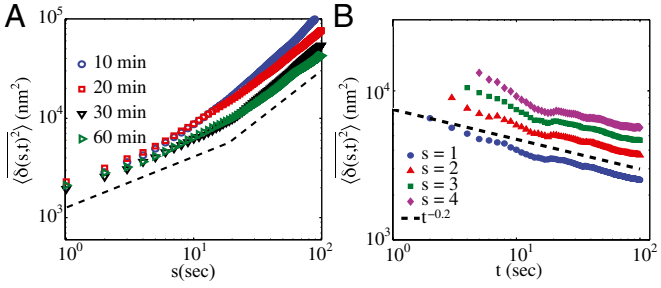

Fig. 5. Effects of vinblastine. (*A*) Average TA-MSD after administration of 5 μM vinblastine in a MIN6 cell. Different symbols represent times (in minutes) the cell was exposed to vinblastine. The dashed line is drawn by hand to indicate the crossover in behavior. During the subdiffusive phase, the anomalous exponents progressively decrease with increasing exposure time: $\alpha = 0.63$, 0.57, 0.52, and 0.45 for 10, 20, 30, and 60 min, respectively. (*B*) Aging behavior as a function of measurement time t (compare with Fig. 2*B*) for different constant s (in seconds) for a MIN6 cell that was exposed to 5 μM vinblastine for 10 min.

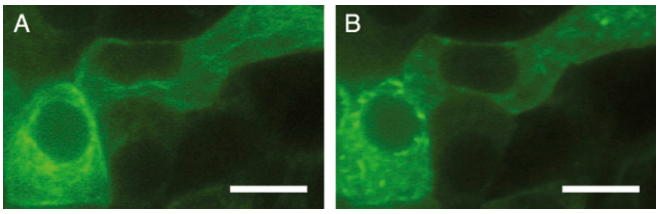

Fig. 6. (*A* and *B*) MIN6 cells before (*A*) and after 20 min of treatment with 5 μM vinblastine (*B*). Microtubules are labeled using CellLight Tubulin-GFP. (Scale bar, 10 μm.) Several cells in a cluster grown on templated glass slides are shown. The microtubules shift from filamentous to short fragments.

crowded environment of the cell or deformation of the filament network when a vesicle is interacting with more than one filament.

Biological Implications. Our results have major implications for pancreatic β-cell function. Insulin granule trafficking following assembly in the Golgi apparatus is a key pathway leading to sustained glucose-stimulated insulin secretion. Whereas individual β-cells in a normal mouse islet contain over 10,000 granules, the maximal rate of exocytosis is estimated to be less than 1 granule per second in physiological conditions (42). For this reason, only a small fraction (<5%) of existing granules must be mobilized for insulin secretion in the initial response to stimulation. The typical response of healthy islets in vitro is biphasic, with an initial sharp rise in insulin within 5 min, followed by a sustained and prolonged second phase that varies according to species and precise experimental conditions (20, 42). Profound changes in this behavior, in particular the loss of the first phase, occur in the diabetic state but remain incompletely understood. Work in islets from diabetic humans suggests the defects lie at the level of granule trafficking and exocytosis (43). Recent studies of insulin secretion have focused on distinct "pools" of granules with varying mobility as the basis for the observed secretion profiles (20).

In contrast, our findings suggest a scheme that combines granule dynamics in the cell interior with those close to the membrane. To see this, we simulate a 2D idealized cell of unit radius (Fig. 7*A*). Ten pores of radius 0.01 units are evenly spaced around the circumference (red circles in Fig. 7*A*); these are motivated by observations of membrane "hot spots" for secretion (44, 45). Particles representing insulin granules are introduced randomly in the cell area with preference toward the center (linearly increasing probability from the outer membrane to the center). These particles move within the cell by a subordinated random walk (with the parameters elucidated above: $H = 0.35$ and $\beta = 0.2$), except within a distance a of a pore (indicated by dashed lines in Fig. 7*A*), where they move by FBM. Close to the membrane there is no trapping, consistent with the observations that led to the notion of "restless" granules (20). Once a particle reaches a pore it is removed irreversibly from the simulation, and we study the flux of particles out of the cell (i.e., the first passage time distribution for exocytosis) as a function of a.

As noted above, relatively few granules are secreted, so arrivals at pores are expected to be rare in comparison with fluctuations in granule positions. It is thus computationally demanding to obtain statistics from direct simulation of this system, especially due to the power-law waiting time distribution of the CTRW that contributes to the subordinated random walk. To overcome this issue, we used steered transition path sampling (46), an algorithm that we recently introduced for enhanced sampling of transient processes that do not obey detailed balance (such as FBM). The idea is that the path ensemble is biased by preferentially selecting otherwise unbiased trajectory segments that make progress toward a goal, and then the physical weighting is restored in computing the first passage time distribution. The trajectory segments that we take to make progress are those with particles that can still

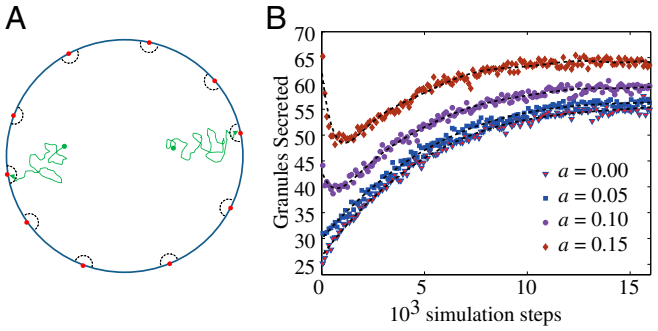

Fig. 7. Subordinated random walk can give rise to biphasic secretion. (*A*) Schematic of the simulation system. (*B*) Flux of particles released from an idealized cell (main text). We measure time from when the channels are opened, so there is no lag in response, in contrast to experimental studies, in which time is usually defined relative to the stimulus.

reach one of the pores within the allotted number of simulation steps (16,000 total for each particle; we generate the FBM steps according to ref. 47 with an average step length of 0.02 units). The bias becomes progressively stronger: As the number of remaining steps decreases, the pressure for particles to be close to pores increases.

The first passage time distributions for several a values are shown in Fig. 7*B*. For $a = 0$ units, the secretion profile exhibits only a slow rise, whereas, for larger a values ($a = 0.1$ units), there is a sharp peak followed by a slow recovery and stabilization. This transition from uni- to biphasic behavior results from the interplay between the two types of dynamics (subordinated and pure FBM). No such transition is observed if only one dynamic is involved. In particular, it is not possible to obtain sustained secretion at a near-constant level (the plateau phase in Fig. 7*B*) without the subordinated dynamics. Anomalous diffusion thus provides a simple physical route to biphasic insulin release that does not require invoking pools of special granules within the cell.

Because metabolic coupling to increased intracellular calcium is only modestly perturbed in β-cell–containing islets from humans with diabetes, one recent study concluded that "aberrant granule docking, decreased Ca^{2+} sensitivity of exocytosis, and reduced insulin release" (ref. 43, p. 1726) were the key issues requiring further study. This study linked genetic susceptibility variants to defects in insulin secretion. Further work is needed to define the defects in granule dynamics in diabetes. The results of ref. 43 in combination with our own suggest that therapies that target insulin granule dynamics from the cytoskeletal network structure to exocytosis could have significant impact in the treatment of type 2 diabetes.

Experimental Methods

Labeling and Imaging Protocols. Syncollin-pEGFP was used to express syncollin, which is targeted to insulin granules in MIN6 cells (21); granules visualized with this construct behave similarly to ones with insulin-GFP fusions (*SI Appendix*, Fig. S12), and this consistency across constructs suggests that the dynamics are native-like. The MIN6 cells were plated on a glass coverslip and incubated for about 1 h in 2 mM glucose before stimulation. All experiments consisted of static incubation performed on a temperature-controlled microscope stage that was maintained at 37 °C. Cells were maintained and perfused with 8 mM glucose and Krebs–Ringer buffer containing 119 mM NaCl, 4.7 mM KCl, 25 mM $NaHCO_3$, 2.5 mM $CaCl_2$, 1.2 mM $MgSO_4$, and 1.2 mM KH_2PO_4.

All image series were acquired using a Yokogawa CSU10 spinning-disk optical confocal scanner and a Roper CoolSnap HQ CCD camera (Roper Scientific), using MetaMorph software (Universal Imaging). Sequential images were taken for 5 min at 1 Hz. EGFP granules were excited with the 488-nm line of an Ar^+/Kr^+ laser (Omnichrome Series 43) with the minimum laser power that would give good signal-to-noise ratio. Fluorescence was collected in an epi-geometry, separated from the excitation laser light (535/40 nm band pass, Chroma) and imaged to the CCD detector. Excessive illumination resulted in premature photobleaching of the sample.

We checked the effect of phototoxicity by imaging the same cells with different relative excitation intensities (25%, 50%, and 100%). In this set of experiments, the power-law scaling for the TA-MSD as a function of lag time (s) and total time (t) is independent of the intensity, with consistent exponents of $\alpha = 0.8$ and $\beta - 1 = -0.37$ (*SI Appendix*, Fig. S12). Therefore, effects from light, if any, do not significantly contribute to the results.

Particle Tracking Algorithm. Diatrack 3.0 (Semasopht) was used for two-dimensional particle tracking of 1 to >100 particles in each image of the measured sequence of insulin granules in live cells as well as both experimental and simulated images of microspheres in solution. Trajectories of insulin granules were recovered after thresholding, background subtraction, and adjustment of parameters such as maximum displacement between successive frames. The resulting single-particle trajectories were analyzed in terms of transport properties and statistics with custom routines written in MATLAB 7.1 (MathWorks). It is important to assess whether the tracking error is the source of apparent subdiffusive behavior (48, 49); we show how the contribution from the tracking error can be assessed in the *SI Appendix* and find that it is negligible in our system.

Controlling for Nonintrinsic Contributions. Because statistical tests for anomalous diffusion rely on the dynamics taking place in a stationary state, we use detrended fluctuation analysis (DFA) (50) to remove any contributions that are not intrinsic to the granule motions (e.g., a slow evolution of the state of the cell). The essential idea is that one fits low-order polynomials to running windows of sequential data and subtracts these polynomial functions from the data to obtain deviations from them. Thus, DFA is a useful tool when one wants to determine the bias of a trend on the scaling properties of a series of measurements without knowing a priori how the trend scales with time. The mathematical protocol of DFA is described briefly in *SI Appendix*. By applying this method to our data, we were able to extend the range of s over which we could linearly fit data before the data get too noisy [compare Fig. 2*A* and *SI Appendix*, Fig. S2 (*Inset*) with *SI Appendix*, Fig. S13]. Also, DFA widened the distribution of the exponents fitted to the first 10% of the data points of the trajectories without significantly shifting its peak (compare *SI Appendix*, Fig. S14 with Fig. S3). Therefore, DFA confirms that the behavior that we describe here is indeed predominantly subdiffusive with some trajectories being diffusive or superdiffusive. Also, in *SI Appendix*, Fig. S15 we see that for the detrended time series, the long tails in the distribution persist.

ACKNOWLEDGMENTS. We thank M. R. Rahimi Tabar for useful discussions and David Chandler for suggesting examination of exchange and persistence times. We also thank the W. M. Keck Foundation for primary support and acknowledge financial and central facilities assistance from the University of Chicago Materials Research Science and Engineering Center (National Science Foundation Grant DMR-0820054). S.M.A.T. was funded by the Human Frontier Science Program organization. N.F.S. thanks the Guggenheim Foundation for support that catalyzed this research.

1. Rothman JE (2002) Lasker Basic Medical Research Award. The machinery and principles of vesicle transport in the cell. *Nat Med* 8(10):1059–1062.
2. Dannies PS (1999) Protein hormone storage in secretory granules: Mechanisms for concentration and sorting. *Endocr Rev* 20(1):3–21.
3. Magde D, Elson E, Webb W (1972) Thermodynamic fluctuations in a reacting system measurement by fluorescence correlation spectroscopy. *Phys Rev Lett* 29:705–708.
4. Kusumi A, Sako Y, Yamamoto M (1993) Confined lateral diffusion of membrane receptors as studied by single particle tracking (nanovid microscopy). Effects of calcium-induced differentiation in cultured epithelial cells. *Biophys J* 65(5):2021–2040.
5. Wiseman PW, Höddelius P, Petersen NO, Magnusson KE (1997) Aggregation of PDGF-beta receptors in human skin fibroblasts: Characterization by image correlation spectroscopy (ICS). *FEBS Lett* 401(1):43–48.
6. Moerner WE (2007) New directions in single-molecule imaging and analysis. *Proc Natl Acad Sci USA* 104(31):12596–12602.
7. Golding I, Cox EC (2006) Physical nature of bacterial cytoplasm. *Phys Rev Lett* 96(9):098102.
8. Kulić IM, et al. (2008) The role of microtubule movement in bidirectional organelle transport. *Proc Natl Acad Sci USA* 105(29):10011–10016.
9. Huet S, et al. (2006) Analysis of transient behavior in complex trajectories: Application to secretory vesicle dynamics. *Biophys J* 91(9):3542–3559.
10. Arcizet D, Meier B, Sackmann E, Rädler JO, Heinrich D (2008) Temporal analysis of active and passive transport in living cells. *Phys Rev Lett* 101(24):248103.
11. Condamin S, Tejedor V, Voituriez R, Bénichou O, Klafter J (2008) Probing microscopic origins of confined subdiffusion by first-passage observables. *Proc Natl Acad Sci USA* 105(15):5675–5680.

12. Dix JA, Verkman AS (2008) Crowding effects on diffusion in solutions and cells. *Annu Rev Biophys* 37:247–263.
13. Metzler R, Klafter J (2000) The random walk's guide to anomalous diffusion: A fractional dynamics approach. *Phys Rep* 339:1–77.
14. Mandelbrot B, Van Ness J (1968) Fractional Brownian motions, fractional noises and applications. *SIAM Rev* 10:422–437.
15. Burov S, Jeon JH, Metzler R, Barkai E (2011) Single particle tracking in systems showing anomalous diffusion: The role of weak ergodicity breaking. *Phys Chem Chem Phys* 13(5):1800–1812.
16. Tolić-Nørrelykke IM, Munteanu EL, Thon G, Oddershede L, Berg-Sørensen K (2004) Anomalous diffusion in living yeast cells. *Phys Rev Lett* 93(7):078102.
17. Weigel AV, Simon B, Tamkun MM, Krapf D (2011) Ergodic and nonergodic processes coexist in the plasma membrane as observed by single-molecule tracking. *Proc Natl Acad Sci USA* 108(16):6438–6443.
18. Weber SC, Spakowitz AJ, Theriot JA (2010) Bacterial chromosomal loci move subdiffusively through a viscoelastic cytoplasm. *Phys Rev Lett* 104(23):238102.
19. Brenner MB, Gromada J, Efanov AM, Bokvist K, Mest HJ (2003) Restoration of first-phase insulin secretion by the imidazoline compound LY374284 in pancreatic islets of diabetic db/db mice. *Ann N Y Acad Sci* 1009:332–340.
20. Seino S, Shibasaki T, Minami K (2011) Dynamics of insulin secretion and the clinical implications for obesity and diabetes. *J Clin Invest* 121(6):2118–2125.
21. Ma L, et al. (2004) Direct imaging shows that insulin granule exocytosis occurs by complete vesicle fusion. *Proc Natl Acad Sci USA* 101(25):9266–9271.
22. Snider J, et al. (2004) Intracellular actin-based transport: How far you go depends on how often you switch. *Proc Natl Acad Sci USA* 101(36):13204–13209.
23. Caspi A, Granek R, Elbaum M (2000) Enhanced diffusion in active intracellular transport. *Phys Rev Lett* 85(26 Pt 1):5655–5658.
24. Seisenberger G, et al. (2001) Real-time single-molecule imaging of the infection pathway of an adeno-associated virus. *Science* 294(5548):1929–1932.
25. Young A (1998) *Spin Glasses and Random Fields* (World Scientific, River Edge, NJ), Vol 12.
26. He Y, Burov S, Metzler R, Barkai E (2008) Random time-scale invariant diffusion and transport coefficients. *Phys Rev Lett* 101(5):058101.
27. Lubelski A, Sokolov IM, Klafter J (2008) Nonergodicity mimics inhomogeneity in single particle tracking. *Phys Rev Lett* 100(25):250602.
28. Deng W, Barkai E (2009) Ergodic properties of fractional Brownian-Langevin motion. *Phys Rev E Stat Nonlin Soft Matter Phys* 79(1 Pt 1):011112.
29. Havlin S, Ben-Avraham D (1987) Diffusion in disordered media. *Adv Phys* 36:695–798.
30. Zwanzig R (1973) Nonlinear generalized Langevin equations. *J Stat Phys* 9:215–220.
31. Burov S, Metzler R, Barkai E (2010) Aging and nonergodicity beyond the Khinchin theorem. *Proc Natl Acad Sci USA* 107(30):13228–13233.
32. Magdziarz M, Weron A, Burnecki K, Klafter J (2009) Fractional Brownian motion versus the continuous-time random walk: A simple test for subdiffusive dynamics. *Phys Rev Lett* 103(18):180602.
33. Chaudhuri P, Berthier L, Kob W (2007) Universal nature of particle displacements close to glass and jamming transitions. *Phys Rev Lett* 99(6):060604.
34. Hedges LO, Maibaum L, Chandler D, Garrahan JP (2007) Decoupling of exchange and persistence times in atomistic models of glass formers. *J Chem Phys* 127(21):211101.
35. Wang B, Anthony SM, Bae SC, Granick S (2009) Anomalous yet Brownian. *Proc Natl Acad Sci USA* 106(36):15160–15164.
36. Valentine MT, Perlman ZE, Mitchison TJ, Weitz DA (2005) Mechanical properties of Xenopus egg cytoplasmic extracts. *Biophys J* 88(1):680–689.
37. Goychuk I (2012) Viscoelastic subdiffusion: Generalized Langevin equation approach. *Adv Chem Phys* 150:187–253.
38. Fogedby HC (1994) Langevin equations for continuous time Lévy flights. *Phys Rev E Stat Phys Plasmas Fluids Relat Interdiscip Topics* 50(2):1657–1660.
39. Meroz Y, Sokolov IM, Klafter J (2010) Subdiffusion of mixed origins: When ergodicity and nonergodicity coexist. *Phys Rev E Stat Nonlin Soft Matter Phys* 81(1 Pt 1):010101.
40. Fletcher LM, Welsh GI, Oatey PB, Tavaré JM (2000) Role for the microtubule cytoskeleton in GLUT4 vesicle trafficking and in the regulation of insulin-stimulated glucose uptake. *Biochem J* 352(Pt 2):267–276.
41. Varadi A, Tsuboi T, Johnson-Cadwell LI, Allan VJ, Rutter GA (2003) Kinesin I and cytoplasmic dynein orchestrate glucose-stimulated insulin-containing vesicle movements in clonal MIN6 beta-cells. *Biochem Biophys Res Commun* 311(2):272–282.
42. Rorsman P, Renström E (2003) Insulin granule dynamics in pancreatic beta cells. *Diabetologia* 46(8):1029–1045.
43. Rosengren AH, et al. (2012) Reduced insulin exocytosis in human pancreatic β-cells with gene variants linked to type 2 diabetes. *Diabetes* 61(7):1726–1733.
44. Watson RT, Pessin JE (2007) GLUT4 translocation: The last 200 nanometers. *Cell Signal* 19(11):2209–2217.
45. Wang Z, Thurmond DC (2009) Mechanisms of biphasic insulin-granule exocytosis - roles of the cytoskeleton, small GTPases and SNARE proteins. *J Cell Sci* 122(Pt 7): 893–903.
46. Guttenberg N, Dinner AR, Weare J (2012) Steered transition path sampling. *J Chem Phys* 136(23):234103.
47. Hosking JRM (1984) Modeling persistence in hydrological time series using fractional differencing. *Water Resour Res* 20:1898–1908.
48. Martin DS, Forstner MB, Käs JA (2002) Apparent subdiffusion inherent to single particle tracking. *Biophys J* 83(4):2109–2117.
49. Weber SC, Thompson MA, Moerner WE, Spakowitz AJ, Theriot JA (2012) Analytical tools to distinguish the effects of localization error, confinement, and medium elasticity on the velocity autocorrelation function. *Biophys J* 102(11):2443–2450.
50. Chen Z, Ivanov PCh, Hu K, Stanley HE (2002) Effect of nonstationarities on detrended fluctuation analysis. *Phys Rev E Stat Nonlin Soft Matter Phys* 65(4 Pt 1):041107.